

Controlled Gate Networks Applied to Eigenvalue Estimation

Max Bee-Lindgren,¹ Zhengrong Qian,² Matthew DeCross,³ Natalie C. Brown,³
Christopher N. Gilbreth,³ Jacob Watkins,² Xilin Zhang,² and Dean Lee²

¹*School of Physics, Georgia Institute of Technology, Atlanta, GA 30332, USA*

²*Facility for Rare Isotope Beams and Department of Physics and Astronomy, Michigan State University, MI 48824, USA*

³*Quantinuum, 303 S. Technology Ct., Broomfield, Colorado 80021, USA*

We introduce a new scheme for quantum circuit design called controlled gate networks. Rather than trying to reduce the complexity of individual unitary operations, the new strategy is to toggle between all of the unitary operations needed with the fewest number of gates. We illustrate our approach using two examples. The first example is a variational subspace calculation for a two-qubit system. We demonstrate an approximately five-fold reduction in the number of two-qubit gates required for computing inner products and Hamiltonian matrix elements. The second example is estimating the eigenvalues of a two-qubit Hamiltonian via the Rodeo Algorithm [1] using a specific class of controlled gate networks called controlled reversal gates. Again, a five-fold reduction in the number of two-qubit gates is demonstrated. We use the Quantinuum H1-2 and IBM Perth devices to realize the quantum circuits. Our work demonstrates that controlled gate networks are a useful tool for reducing gate complexity in quantum algorithms for quantum many-body problems.

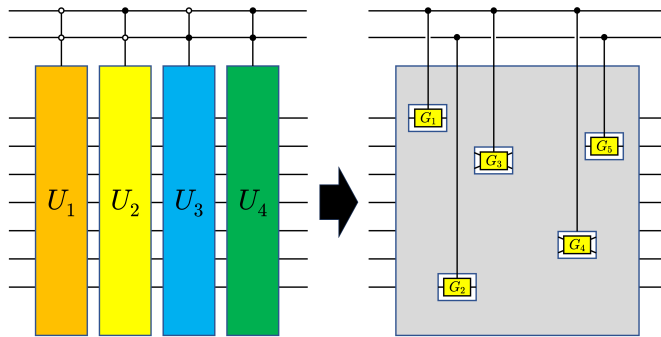


FIG. 1. Example of a controlled gate network. The left side shows a circuit using two ancilla qubits to toggle between four possible unitary operators, U_1, U_2, U_3, U_4 . The filled (open) dot means that the controlled operator is actuated when the attached ancilla is in the $|1\rangle$ ($|0\rangle$) state. The right side achieves the same results using a controlled gate network. Each of the transformation gates G_i act on a small number of qubits. U_1 corresponds to no G_i actuated, U_2 corresponds to actuating $\{G_1, G_3, G_4\}$, U_3 corresponds to $\{G_2, G_5\}$, and U_4 corresponds to $\{G_1, G_2, G_3, G_4, G_5\}$.

INTRODUCTION

Many quantum circuits involve combinations of unitary operators executed in sequence, with logical control directed by one or more auxiliary registers [2–5]. In order to minimize circuit complexity, many promising techniques and strategies have been developed [6–12]. For circuits with controlled unitary operations, the conventional approach is to reduce the gate complexity of each controlled unitary operator as much as possible. During the transpilation stage, simplifications between circuit blocks may be found and exploited, such as cancelling neighboring CNOT gates. However, this alone does not suggest how one ought to design circuits intentionally such that cancellations are common.

Here we present a different approach in which all the unitary operations needed are viewed as a connected network, and the transformations between the operations are optimized. We define a controlled gate network to be a set of controlled operations such that any two operations can be transformed into each other by inserting or removing a small number of gates that we call transformation gates. An example of a controlled gate network is illustrated in Fig. 1. The left side shows a circuit using two ancilla qubits to toggle between four possible unitary operators, U_1, U_2, U_3, U_4 . The right side achieves the same results using a controlled gate network. Each of the transformation gates G_i act on a small number of qubits, and the ancilla qubits control the transformation gates. Further details are given in the figure caption.

Controlled gate networks can be very useful for quantum algorithms that repeatedly use controlled gates. Examples include linear combinations of unitaries for Hamiltonian simulation and quantum signal processing [2, 13], phase estimation [14–17], imaginary time evolution [18, 19], and variational subspace methods [20–24]. In particular, controlled operations that are closely related to each other are well-suited for these networks, as only a small number of gates may be used to change between them. The application to variational subspace methods is particularly noteworthy. There a single auxiliary qubit can be used to prepare the superposition of any two variational states generated by the controlled gate network. These superpositions can then be used to determine all the inner products and Hamiltonian matrix elements needed.

Our purpose of this work is to introduce the concept of a controlled gate network and show how it can reduce the number of gates in circuits when repeated controlled operations with similar structures are required. We illustrate with two specific examples that are analyzed in detail. The first example is a variational subspace calculation for a two-qubit system. The task requires computing inner products and Hamiltonian matrix elements for state vectors produced using unitary transformations with different input parameters. We show that the standard approach requires 64 CNOT gates and 82 single qubit gates, but the controlled gate network approach requires only 13 CNOT gates and 21 single qubit gates.

The second controlled gate network example we discuss is called controlled reversal gates. Controlled reversal gates reverse the flow of time in Hamiltonian simulations using anticommuting operators and an auxiliary qubit as a switch. This functionality makes it valuable for eigenvalue estimation methods such as the Rodeo Algorithm. We will see that controlled reversal gates reduce the number of two-qubit entangling gates required for our system by a factor of 5 as compared with an approach using standard controlled gates. These calculations are carried out on the IBM Perth and Quantinuum H1-2 machines. In the following, we present the implementation of the Rodeo Algorithm with controlled reversal gates on the IBM Perth and Quantinuum H1-2 machines.

VARIATIONAL SUBSPACE CALCULATIONS USING CONTROLLED GATE NETWORKS

In the quantum approximate optimization algorithm (QAOA) [25–27], one approximates the ground state of a Hamiltonian H using a variational ansatz of the form,

$$|\vec{\epsilon}, \vec{\lambda}\rangle = \exp(-i\epsilon_N H_I) \exp(-i\lambda_N H) \cdots \exp(-i\epsilon_1 H_I) \exp(-i\lambda_1 H) |\psi_I\rangle, \quad (1)$$

where $|\psi_I\rangle$ is the ground state of some trivial initial Hamiltonian, H_I . The parameters $\vec{\epsilon}$ and $\vec{\lambda}$ are then optimized to give the lowest expectation value $\langle \vec{\epsilon}, \vec{\lambda} | H | \vec{\epsilon}, \vec{\lambda} \rangle$ ¹. However, this single-vector ansatz for the ground state may not be sufficient. The variational approximation can be improved if we allow for linear combinations of variationally-optimized QAOA vectors $|\vec{\epsilon}^{(i)}, \vec{\lambda}^{(i)}\rangle$. Variational optimization using a subspace rather than a single vector allows for the mixing of configurations that explicitly break symmetries of the Hamiltonian such as rotational invariance, particle number conservation, or internal flavor symmetries. The underlying symmetry is restored by allowing for linear combinations of the individual configurations. This strategy of explicit symmetry breaking and symmetry restoration is widely used in nuclear physics [28–33]. In order to perform a variational subspace calculation, one needs to be able to compute inner products, $\langle \vec{\epsilon}^{(i)}, \vec{\lambda}^{(i)} | \vec{\epsilon}^{(j)}, \vec{\lambda}^{(j)} \rangle$ and Hamiltonian matrix elements $\langle \vec{\epsilon}^{(i)}, \vec{\lambda}^{(i)} | H | \vec{\epsilon}^{(j)}, \vec{\lambda}^{(j)} \rangle$ between pairs of QAOA states. One can then solve the generalized eigenvalue problem using classical post-processing to find the ground state of H within the projected subspace [21, 24, 34–37].

To illustrate with a simple example, we consider a two-qubit system where the Hamiltonian H corresponds to a Heisenberg model,

$$H = aX_j X_k + bY_j Y_k + cZ_j Z_k. \quad (2)$$

If we take the initial Hamiltonian to be $H_I = -\sum_i X_i$, then each layer of the QAOA product will produce a product of exponentials of the form,

$$N(\alpha, \beta, \gamma, \delta) = \exp(i\delta X_j) \exp(i\delta X_k) \exp[i(\alpha X_j X_k + \beta Y_j Y_k + \gamma Z_j Z_k)], \quad (3)$$

with real parameters $\alpha, \beta, \gamma, \delta$. In order to perform the variational subspace calculations using such QAOA states, we need to construct superpositions of $|A\rangle \equiv N(\alpha, \beta, \gamma, \delta) |\psi_I\rangle$ and $|B\rangle \equiv N(\alpha + \Delta\alpha, \beta + \Delta\beta, \gamma + \Delta\gamma, \delta + \Delta\delta) |\psi_I\rangle$, where $|\psi_I\rangle$ is the initial state of the system. Let us first show how this is done efficiently using a controlled gate network.

We can implement $N(\alpha, \beta, \gamma, \delta)$ and $N(\alpha + \Delta\alpha, \beta + \Delta\beta, \gamma + \Delta\gamma, \delta + \Delta\delta)$ using a controlled gate network as shown in Fig. 2. We are using the implementation of $N(\alpha, \beta, \gamma, \delta)$ described in Ref. [38]. The transformation gates are highlighted in yellow. When the transformation gates are not included, the circuit gives $N(\alpha, \beta, \gamma, \delta)$. When the transformation gates are included, the circuit equals $N(\alpha + \Delta\alpha, \beta + \Delta\beta, \gamma + \Delta\gamma, \delta + \Delta\delta)$. By using one ancilla qubit to control all of the transformation gates, we can construct an arbitrary superposition of $|A\rangle \equiv N(\alpha, \beta, \gamma, \delta) |\psi_I\rangle$ and $|B\rangle \equiv N(\alpha + \Delta\alpha, \beta + \Delta\beta, \gamma + \Delta\gamma, \delta + \Delta\delta) |\psi_I\rangle$, where $|\psi_I\rangle$ is the initial state of the system.

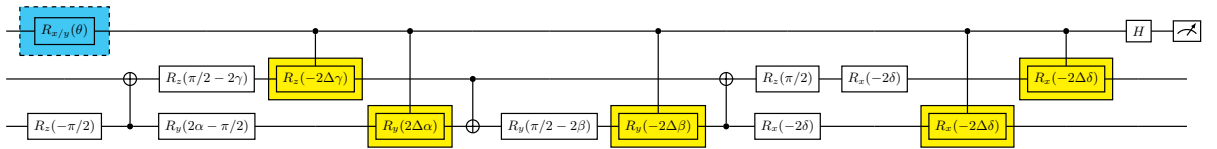


FIG. 2. Controlled gate network for our variational subspace calculation example. The transformation gates are highlighted in yellow. When the transformation gates are not included, the circuit gives $N(\alpha, \beta, \gamma, \delta)$. When the transformation gates are included, the circuit equals $N(\alpha + \Delta\alpha, \beta + \Delta\beta, \gamma + \Delta\gamma, \delta + \Delta\delta)$. By using one ancilla qubit to control all of the transformation gates, we can construct an arbitrary superposition of $N(\alpha, \beta, \gamma, \delta)$ and $N(\alpha + \Delta\alpha, \beta + \Delta\beta, \gamma + \Delta\gamma, \delta + \Delta\delta)$.

By aligning \hat{n} with y and x axes in the $R_{\hat{n}}(\theta)$ gate and performing a measurement on the ancilla qubit, we can deduce the real and imaginary parts of the inner product $\langle A|B\rangle$ from the measurement probabilities of the $|0\rangle$ and $|1\rangle$ states. We can apply the same technique to calculate the matrix elements for the Hamiltonian, $\langle A|H|B\rangle$, and their complex conjugates. This is done by decomposing H into a sum of unitary operators such as strings of Paul matrices, $H = \sum_k U_k$. We then replace $|B\rangle$ in the description above with $U_k |B\rangle$ for each k . If we decompose and transpile the circuit in Fig. 2 into native gates for the IBM system, we get the circuit shown in Fig. 3. A total of 13 CNOT gates and 21 single qubit gates are required.

¹ These parameters are typically labeled $\vec{\beta}$ and $\vec{\gamma}$ in the QAOA literature; however, these symbols have already been used elsewhere in the text so they have been relabeled here for clarity.

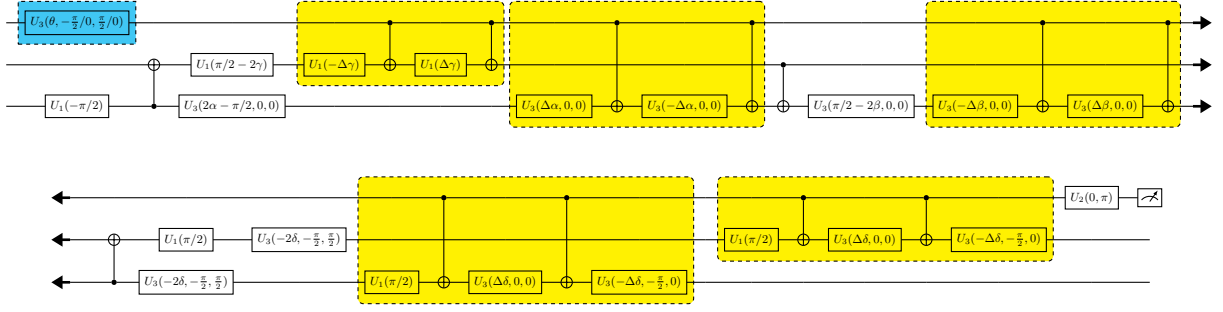


FIG. 3. This is the fully decomposed and transpiled version for the circuit in Fig. 2 using gates native to the IBM system. A total of 13 CNOT gates and 21 single qubit gates are required.

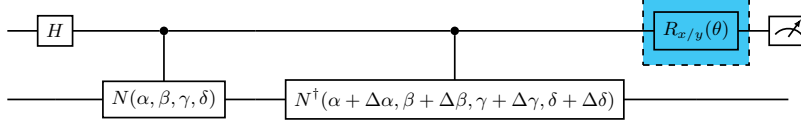


FIG. 4. Standard Hadamard test circuit for computing the real and imaginary parts of the inner product $\langle A|B\rangle$.

We can now compare with the standard approach for calculating $\langle A|B\rangle$ using a Hadamard test [21]. The corresponding circuit is shown in Fig. 4. If we decompose and transpile the circuit in Fig. 4 into native gates for the IBM quantum devices, we get the circuit shown in Fig. 5. A total of 64 CNOT gates and 82 single qubit gates are required. We conclude that the controlled gate network approach substantially more efficient than the standard approach. The reduction in the number of gates is a factor of about 5 for the CNOT gates and a factor of about 4 for the single qubit gates.

RODEO ALGORITHM WITH CONTROLLED REVERSAL GATES

There are several well-known quantum computing algorithms that measure eigenvalues of a Hermitian operator H by means of time evolution controlled by an auxiliary quantum register. An important example is the class of phase estimation algorithms, which includes standard phase estimation [15, 16, 39] and iterative quantum phase estimation [14, 17]. The Rodeo Algorithm is another recently introduced method that uses controlled time evolution [1]. It is an iterative algorithm that uses destructive interference to suppress eigenvectors with eigenvalues different from a desired “target” eigenvalue. The Rodeo Algorithm was shown to have exponentially improved scaling in terms of the precision Δ for preparing eigenstates [1], compared to quantum phase estimation and adiabatic evolution [40, 41].

The first implementation of the Rodeo Algorithm was performed in Ref. [42] for a single qubit Hamiltonian. However, the use of controlled time evolution makes the implementation for a multi-qubit system significantly more difficult, especially on existing noisy quantum devices. In order to reduce the number of two qubit operations, in this work we use controlled reversal gates that allow one to flip the direction of time evolution using an auxiliary qubit.

Let us consider the two-qubit Hamiltonian

$$H_{\text{obj}} = c_1 X_1 Z_2 + c_2 Z_1 X_2 \quad (4)$$

where $c_1, c_2 \in \mathbb{R}$ and X_i and Z_i are the Pauli operators on qubit i . Following the notation of Ref. [1, 42], we call H_{obj} the “object Hamiltonian”. We take the coefficients to be $c_1 = 2.5$ and $c_2 = 1.5$, and the Hamiltonian has four eigenvalues $\pm(c_1 \pm c_2)$. The quantum circuit implementing the time evolution of H_{obj} is shown in Fig. 6.

Each cycle of the Rodeo Algorithm uses a controlled time evolution with a random time t sampled from a normal distribution with zero mean and standard deviation σ set by the user. For any given rodeo cycle, the measurement of 0 for the ancilla corresponds to a successful measurement. Let $|\psi_I\rangle$ be the initial state and let $|E_k\rangle$ denote the energy eigenstates of H_{obj} with energy E_k . If we apply n cycles of the Rodeo Algorithm and average over many random trials, the probability of success for all n cycles at target energy E (a free parameter) is

$$P_n(E) = \sum_k \frac{\left[1 + e^{-(E-E_k)^2 \sigma^2 / 2}\right]^n |\langle E_k | \psi_I \rangle|^2}{2^n}. \quad (5)$$

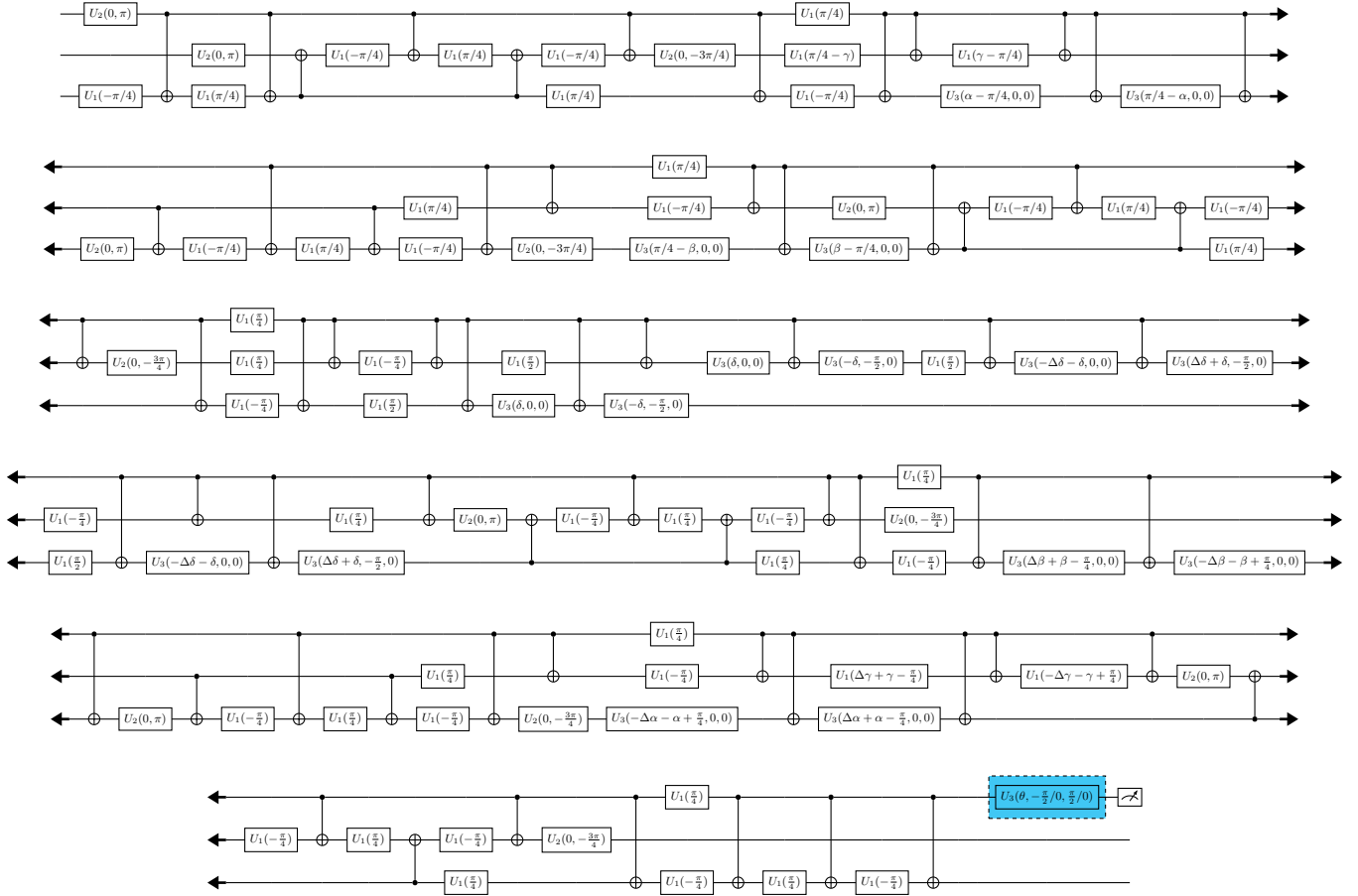


FIG. 5. The fully decomposed and transpiled version for the circuit in Fig. 4 using gates native to the IBM quantum devices. A total of 64 CNOT gates and 82 single qubit gates are required.

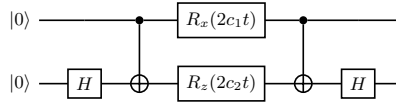


FIG. 6. Quantum circuit implementing the two-qubit unitary $\exp\{-iH_{\text{obj}}t\}$, where H_{obj} is given by Eq. (4).

We see that there are peaks centered at each energy eigenvalue E_k where the initial state has nonzero overlap with $|E_k\rangle$. We also see that there is a constant background value of $\frac{1}{2^n}$ for values of E that are significantly further than σ^{-1} away from all energy eigenvalues. Thus, repeated cycles will indicate peaks whenever E is chosen within $O(\sigma^{-1})$ of some E_k such that $|\langle E_k|\psi_I\rangle|^2$ is not vanishingly small.

When implemented using the IBM Qiskit transpiler [43] under the assumption of full connectivity between all qubits, directly controlling the time evolution of the circuit in Fig. 6 with an ancilla qubit requires a total of 20 CNOT gates. For the Quantinuum H1-2 device at the time of this experiment, the two-qubit entangling gate was the R_{ZZ} gate with angle $\pi/2$, and one needs 20 R_{ZZ} gates for the analogous circuit. With only partial connectivity, the number of two-qubit entangling gates grows even larger. For three cycles of the Rodeo Algorithm, we therefore need 60 two-qubit entangling gates. For five cycles of the Rodeo Algorithm, we need 100 two-qubit entangling gates. For systems with more than two qubits, the problem is even more severe since the number of two-qubit gates will also scale with the number of Trotter-Suzuki time steps.

Controlled reversal gates can reduce these circuit complexities. We define a reversal gate R to be a product of single qubit gates $R = G_1 G_2 \cdots G_N$ that anticommutes with some subset of terms in the Hamiltonian, and write H_R to be the part of the Hamiltonian anticommuteing with R . If the Hamiltonian is written as a sum of products of Pauli gates, then it is straightforward to partition the terms in the Hamiltonian so that each partition has some corresponding reversal gate. A controlled reversal gate C_R is the controlled version of R , i.e., $C_R = C_{G_1} C_{G_2} \cdots C_{G_N}$. Since $R H_R R^\dagger = -H_R$, and since $-H$ generates a backwards

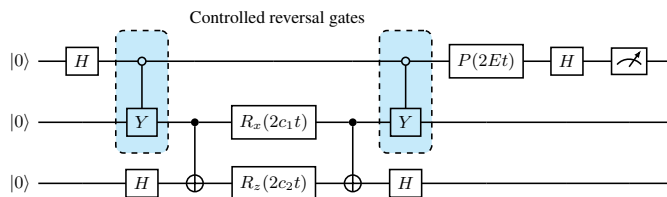


FIG. 7. Circuit diagram for one cycle of the Rodeo Algorithm on the two-qubit system. The ancilla is shown on top, and the controlled reversal gates are the pair of C_Y gates. The phase gate $P(2Et)$ multiplies a phase of $\exp(i2Et)$ to the $|1\rangle$ state of the ancilla and cancels the relative phase produced by the controlled time evolution for an eigenstate with energy E .

evolution of H , C_R allows one to toggle the flow of time forwards and backwards, depending on the state of the auxiliary register.

The relative phase between the states entangled with the ancilla states $|0\rangle$ and $|1\rangle$ is the physically relevant quantity, while any global phase is irrelevant. When using controlled reversal gates, it is desirable that the approximate time evolution operator $\tilde{U}(t)$ is time-reversal symmetric, in the sense of $\tilde{U}(-t) = \tilde{U}(t)^\dagger$. This ensures that $\tilde{U}(t)$ and $\tilde{U}(-t)$ have the same stationary states. For our two-qubit Hamiltonian example, the evolution is exact and thus this symmetry is satisfied. For Hamiltonian simulation using the Trotter approximation, the symmetry is satisfied if the single Trotter step $\mathcal{P}(t)$ satisfies $\mathcal{P}(-dt) = \mathcal{P}(dt)^{-1}$. This is automatically satisfied by the recursive Trotter-Suzuki formulas, particularly at second order [44, 45].

The controlled reversal gates implement forward or backward time evolution depending on the ancilla state. Therefore, the relative phase between the two states evolves at twice the rate as the standard controlled- \tilde{U} setup, and we can reduce the number of Trotter steps by a factor of two. This feature by itself provides a two-fold performance advantage. For this reason, the computational advantage in using controlled reversal gates with the rodeo algorithm is at least a factor of two, independent of the details of the Hamiltonian. For the Hamiltonian that we consider here, we can find a reversal gate that commutes with all of the terms in the Hamiltonian, resulting in an even greater computational advantage. For the general case, however, we will need break up the Hamiltonian into pieces and apply the appropriate reversal gate for each piece. If we are using the Trotter approximation to implement time evolution, then this break up of the Hamiltonian is already done, and the application of controlled reversal gates for the time evolution is straightforward.

IDENTIFYING ENERGY EIGENVALUES

We now use controlled reversal gates and the Rodeo Algorithm to compute the energy spectrum of H_{obj} from Eq. (4). We note that the single-qubit Pauli Y_1 anticommutes with H_{obj} and thus choose C_{Y_1} as our controlled reversal gate (C_{Y_2} is equally valid). One cycle of the Rodeo Algorithm for our system is shown in Fig. 7. It consists of a pair of controlled reversal gates controlled by a single ancilla qubit followed by mid-circuit measurement. By implementing the controlled reversal gates, we are able to reduce the number of CNOT gates for each rodeo cycle from 20 to 4.

Our search for the energy eigenvalues consists of three separate “energy scans,” referring to a collection of cycles with same resolution σ but varying target energy E . Each subsequent scan has a finer resolution and smaller range. The purpose of our coarse-grained first scan ($\sigma = 4$) is to locate all possible regions of the energy spectrum with energy eigenvalue peaks. We identify any region with a success probability well above the average background value of $\frac{1}{2^n}$ as a candidate for the more focused second scan with finer resolution ($\sigma = 14$). The second scan is used to more finely determine the structure of the peaks associated with each energy eigenvalue. The third and final scan uses the finest resolution ($\sigma = 24$) in order to accurately determine the center of each eigenvalue peak. The final scan consists of about twenty circuits spanning a narrow region around each peak identified in the second scan.

IBM AND QUANTINUUM RESULTS

We have performed the Rodeo Algorithm using three cycles and five cycles on the IBM Perth machine and five cycles on the Quantinuum H1-2 machine. For all cases, we follow the same procedure. The initial state is $|\psi_I\rangle = |00\rangle$. The first energy scan is performed with $\sigma = 4$, the second scan with $\sigma = 14$, and third and final scan with $\sigma = 24$.

Let N_c be the number of distinct circuits implemented in a given scan, each with a unique set of Gaussian random values for the times. Let N_s be the number of shots used for each circuit. The observed success probability $P_n(E)$ for n cycles equals the number of successful measurements of 0’s for all n cycles divided by $N_s N_c$. For all the circuits performed in this study,

we use $N_s = 1024$. For the first scan we take $N_c = 5$, for the second scan $N_c = 2$, and for the final scan $N_c = 1$. Since we are drawing from a binomial distribution, we can estimate that the one-standard-deviation statistical error for our measurement of $P_n(E)$ will be $\epsilon_n(E) = \sqrt{P_n(E)[1 - P_n(E)]/(N_s N_c)}$. Since the success probability has a peak at each energy eigenvalue, E_k , we can fit a Gaussian function to each peak in the final scan data and determine the eigenvalues E_k .

The results for three cycles of the Rodeo Algorithm on IBM Perth are shown in the third column of Table I. The success probabilities versus energy are shown in Fig. 8. The curve with the dashed lines shows the exact analytical results for $\sigma = 4$. We also show the results for the first scan using a noiseless classical simulation. The peak success probabilities for the first scan are about 15% lower than the values from the noiseless classical simulations. The average CNOT error for the portion of the IBM Perth device used is about 1%, and we expect that the largest source of noise is due to the 12 CNOT gates needed for each circuit. When compared with the exact results, the RMS deviation for the four eigenvalues is 0.010, which is 0.12% of the full range of the energy spectrum. Meanwhile, the RMS value for the one-sigma uncertainties of the four eigenvalues is 0.006 or 0.07% of the full energy range. We observe that the relative accuracy of the energy measurement is far better than the fidelity of the quantum circuits and is a striking example of the strong noise resilience of the Rodeo Algorithm.

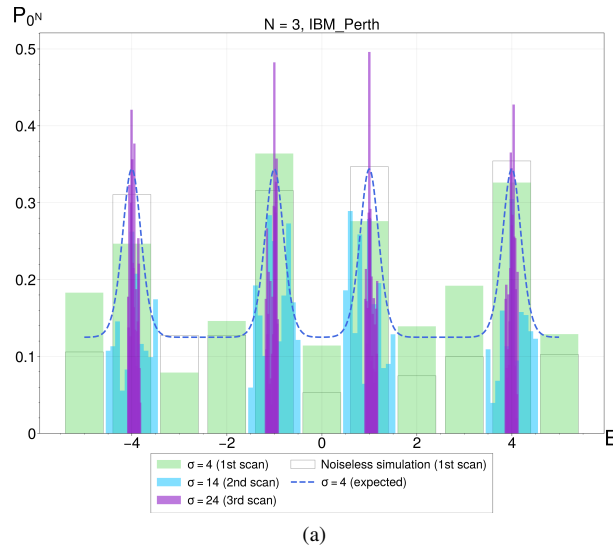


FIG. 8. Success probabilities corresponding to three scans of the rodeo algorithm for the IBM Perth system with three cycles. The dashed line is the expected success probability from classical calculations of the first scan, and the white boxes are noiseless simulations at the energies of first scan.

The success probability versus energy for five cycles on IBM Perth are shown in Panel (a) of Fig. 9. In this case we see that the peak success probabilities for the first scan are about 30% lower than the values from the noiseless classical simulations — a significant reduction in performance. In this case we are using 20 CNOT gates. The results of the fit for five cycles on IBM Perth are shown in the fourth column of Table I. When compared with the exact results, the RMS deviation for the four eigenvalues is 0.004, which is 0.05% of the full range of the energy spectrum. The RMS value for the one-sigma uncertainties of the four eigenvalues is 0.003 or 0.04% of the full energy range. We observe that the relative accuracy of the energy measurement is many orders of magnitude better than the roughly 30% error rate for the quantum circuits.

The success probability versus energy for five cycles on the Quantinuum H1-2 are shown in Panel (b) of Fig. 9 [46]. In contrast with the IBM Perth results, the peak success probabilities for the first scan are close to those from the noiseless classical simulations, as one might expect due to the much better gate fidelities for the Quantinuum H1-2. The error rate for the R_{ZZ} gate at the time of the experiment was 0.3%, and the error rate for the 20 R_{ZZ} gates needed for five cycles explains the approximately 5% reduction in peak heights compared with noiseless simulations. The results of the fit for five cycles on the Quantinuum H1-2 are shown in the fifth column of Table I. When compared with the exact results, the RMS deviation for the four eigenvalues is 0.005, which is 0.06% of the full range of the energy spectrum. The RMS value for the one-sigma uncertainties of the four eigenvalues is 0.003 or 0.03% of the full energy range. We again see that the accuracy of the energy measurement is several orders of magnitude better than the roughly 5% error rate for the quantum circuits.

The noise robustness of the Rodeo Algorithm comes from the fact that it implements a simple strategy of reducing the spectral weight of eigenstates with the wrong energy [42]. While noise will reduce the spectral weight of the desired eigenstate, the associated eigenvalue peak will still be visible if the peak height is not reduced below the random background level. Therefore, we expect the peak height to be reduced by noise, but the peak location should be unaffected. This is clearly demonstrated in the

results described above. See the Supplemental Materials for a detailed analysis using a simple noise model.

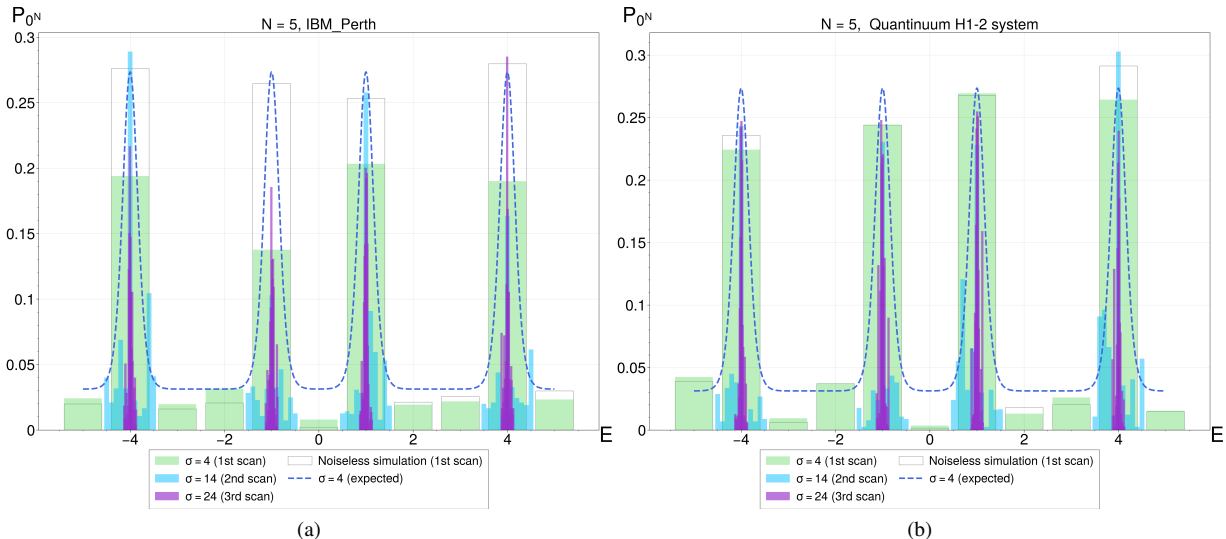


FIG. 9. Success probabilities corresponding to three scans of the Rodeo Algorithm for (a) the IBM Perth system with five cycles and (b) the Quantinuum H1-2 system with five cycles. The dashed line is the expected success probability from classical calculations of the first scan, and the white boxes are noiseless simulations at the energies of first scan.

DISCUSSION AND OUTLOOK

We have introduced a new scheme for quantum circuit design called controlled gate networks. A controlled gate network is a set of controlled operations such that any two operations can be transformed into each other by inserting or removing a small number of gates called transformation gates. Rather than reducing the complexity of individual unitary operations, the goal is to toggle between the required unitary operations with the fewest number of gates.

We have demonstrated the method with two examples. The first is a variational subspace calculation for a two-qubit system. The second example is estimating the eigenvalues of a two-qubit Hamiltonian using the Rodeo Algorithm. For the two examples presented here, the reduction in gate complexity using controlled gate networks is substantial. We found an approximately five-fold reduction in the number of CNOT gates for the two-qubit variational subspace example. We have also demonstrated a five-fold reduction in the number of CNOT gates need for the two-qubit Rodeo Algorithm implementation. In the Supplemental Materials, we show that the generalization of the Rodeo Algorithm calculation for N qubits yields an even more substantial factor of 20 reduction in the number of two-qubit entangling gates for large N when using controlled reversal gates.

Controlled gate networks represent a new paradigm for quantum circuit design where a controlling qubit is used to efficiently transform from one unitary operation to another unitary operation with a similar structure. These controlled unitary operations are common in quantum state preparation algorithms for quantum many-body systems. We have explored two examples in this work and found substantial reductions in gate complexity. We anticipate that controlled gate networks can play a prominent role in improving the efficiency for these applications and as well as many other quantum algorithms.

We have also demonstrated that the Rodeo Algorithm with controlled reversal gates is a practical and efficient method for eigenvalue estimation on current quantum devices. In order to determine energy eigenvalues accurately, the Rodeo Algorithm needs only to be able to distinguish the peak associated with an energy eigenvalue above the background level of $\frac{1}{2^n}$. Once this threshold criterion is reached, the accuracy of the Rodeo Algorithm for determining energy eigenvalue is set by the sharpness of the energy eigenvalue peaks in Eq. (5). The width of the peak scales as $(\sqrt{n}\sigma)^{-1}$, where n is the number of cycles and σ is the standard deviation of the Gaussian random times. We have demonstrated here that with $n = 3$ cycles of the Rodeo Algorithm and $\sigma = 24$, we can resolve the energy eigenvalue with an error of about 0.010 on IBM Perth, or $0.42(\sqrt{n}\sigma)^{-1}$. With $n = 5$ cycles of the Rodeo Algorithm and $\sigma = 24$, we can resolve the energy eigenvalue with an error of about 0.005 on IBM Perth, or $0.27(\sqrt{n}\sigma)^{-1}$; on Quantinuum H1-2, we can resolve the energy eigenvalue with an error of about 0.006, or $0.32(\sqrt{n}\sigma)^{-1}$.

	Exact	IBM Perth Three Cycles	IBM Perth Five Cycles	Quantinuum H1-2 Five Cycles
$ \psi_0\rangle$	-4	-4.0022(49)	-4.0006(42)	-3.9982(21)
$ \psi_1\rangle$	-1	-0.9829(56)	-0.9927(40)	-1.0083(39)
$ \psi_2\rangle$	1	1.0007(26)	1.0008(19)	1.0028(22)
$ \psi_3\rangle$	4	4.0093(84)	3.9982(25)	4.0036(17)

TABLE I. Energy eigenvalue estimates from the final pass of the Rodeo Algorithm with differing numbers of cycles on different devices. The exact values are provided for comparison.

Acknowledgements We are grateful for discussions with Joey Bonitati, Eli Chertkov, Michael Foss-Feig, Gabriel Given, David Hayes, Caleb Hicks, Brian Neyenhuis, and Danny Samuel. We also thank Jay Gambetta and IBM Q for the research accounts and access to hardware. We acknowledge financial support from the U.S. Department of Energy through grants DE-SC0021152, DE-SC0013365, DE-SC0023658, DE-SC0024586, DE-SC0023175 and the U.S. National Science Foundation through the grant PHY-2310620 and the Graduate Research Fellowship Program through the grant DGE-1848739. This research used resources of the Oak Ridge Leadership Computing Facility, which is a DOE Office of Science User Facility supported under Contract DE-AC05-00OR22725.

SUPPLEMENTAL MATERIALS

Success probabilities

For each rodeo cycle, the random times t are selected according to the normalized Gaussian distribution

$$p(t) = \frac{1}{\sqrt{2\pi}\sigma} e^{-\frac{t^2}{2\sigma^2}}. \quad (\text{S1})$$

If our initial is an eigenstate with energy E_k , then the success probability for one cycle with target energy E is

$$\frac{1}{\sqrt{2\pi}\sigma} \int dt e^{-\frac{t^2}{2\sigma^2}} \cos^2[(E_k - E)\frac{t}{2}] = \frac{1 + e^{-(E_k - E)^2 \sigma^2 / 2}}{2}, \quad (\text{S2})$$

and the probability of success for all n cycles is

$$\left[\frac{1 + e^{-(E_k - E)^2 \sigma^2 / 2}}{2} \right]^n. \quad (\text{S3})$$

Let us now consider an initial state $|\psi_I\rangle$, which we can decompose into energy eigenstates

$$|\psi_I\rangle = \sum_k \langle E_k | \psi_I \rangle |E_k\rangle. \quad (\text{S4})$$

With this initial state, the success probability after n rodeo cycles will then equal

$$P_n(E) = \sum_k \frac{\left[1 + e^{-(E_k - E)^2 \sigma^2 / 2} \right]^n |\langle E_k | \psi_I \rangle|^2}{2^n}. \quad (\text{S5})$$

Noisy Hamiltonian evolution

Consider a simple noise model in which the circuit still implements Hamiltonian time evolution for each cycle, but noise in the Hamiltonian shifts the energy eigenvalues E_k by some amount $\delta E_{k,i}$ for the i th cycle of the algorithm, where $\delta E_{k,i}$ is random shot-to-shot and is independently distributed between cycles. To first order in the noise, we assume that the eigenvectors $|E_k\rangle$ are unchanged. The noisy success probability can be obtained by averaging $P_n(E)$ over the distribution $p(\delta E_{k,n})$ of the noise:

$$P_{n,\text{noisy}}(E) = \sum_k \frac{|\langle E_k | \psi_I \rangle|^2}{2^n} \prod_{i=1}^n \int d(\delta E_{k,i}) p(\delta E_{k,i}) \left[1 + e^{-(E_k + \delta E_{k,i} - E)^2 \sigma^2 / 2} \right]. \quad (\text{S6})$$

In the simple case where $\delta E_{k,i}$ is Gaussian distributed with mean 0 and standard deviation ε_k , then $p(\delta E_{k,i}) = \frac{1}{\sqrt{2\pi\varepsilon_k^2}} e^{-(\delta E_k)^2 / (2\varepsilon_k^2)}$ and

$$\int d(\delta E_{k,i}) p(\delta E_{k,i}) \left[1 + e^{-(E_k + \delta E_{k,i} - E)^2 \sigma^2 / 2} \right] = 1 + \frac{e^{-(E_k - E)^2 \sigma^2 / [2(1 + \varepsilon_k^2 \sigma^2)]}}{\sqrt{1 + \varepsilon_k^2 \sigma^2}}. \quad (\text{S7})$$

The centers of the peaks thereby remain at E_k . When the eigenenergies are well-separated, the peak height at $E = E_k$ is reduced by a factor of $\left[1 + \frac{1}{\sqrt{1 + \varepsilon_k^2 \sigma^2}} \right]^n / 2^n$, which gives exponential suppression in the number n of cycles. When $\varepsilon_k^2 \sigma_k^2 \ll 1$, one obtains

$$P_{n,\text{noisy}}(E_k) \approx |\langle E_k | \psi_I \rangle|^2 \left[1 - \varepsilon_k^2 \sigma^2 / 4 \right]^n. \quad (\text{S8})$$

One can also consider the case when $\delta E_{k,i} = \delta E_k$ is independent shot-to-shot, but the same for all cycles. This might, for instance, reflect slowly-varying coherent errors arising from calibration inaccuracies. Assuming sufficient sampling that averages over the error distribution,

$$P_{n,\text{noisy}}(E) = \sum_k \frac{|\langle E_k | \psi_I \rangle|^2}{2^n} \int d(\delta E_k) p(\delta E_k) \left[1 + e^{-(E_k + \delta E_k - E)^2 \sigma^2 / 2} \right]^n. \quad (\text{S9})$$

For a Gaussian error distribution, this will again leave the centers of the peaks unchanged. To find the suppression of the peak height, one can set $E = E_k$ and perform the binomial expansion and the integration. Assuming the peaks are well-separated, one obtains

$$P_{n,\text{noisy}}(E_k) \approx \frac{|\langle E_k | \psi_I \rangle|^2}{2^n} \sum_m \binom{n}{m} \frac{1}{\sqrt{1 + m\varepsilon^2\sigma^2}}. \quad (\text{S10})$$

Assuming $m\varepsilon_k^2\sigma^2 \ll 1$, then to lowest order one obtains

$$P_{n,\text{noisy}}(E_k) \approx |\langle E_k | \psi_I \rangle|^2 [1 - n\varepsilon_k^2\sigma^2/4]. \quad (\text{S11})$$

In this case, one sees only a linear decay of the peak height in the number of rodeo cycles.

Generalization to the N qubit system

We now consider the performance of the Rodeo Algorithm for the generalization of our Hamiltonian to a one-dimensional chain with N qubits,

$$H_{\text{obj}} = \sum_{n=0}^{N-1} (c_1 X_n \otimes Z_{n+1} + c_2 Z_n \otimes X_{n+1}). \quad (\text{S12})$$

For notational convenience we assume that N is even. We perform the time evolution using the second-order Trotter-Suzuki approximation with time step dt [44, 45]. This involves alternating the time evolution of the even- n and odd- n terms in Eq. (S12). If the N -qubit system is evolved for time duration σ , then the total number of two-qubit exponentials required is $N\sigma/dt + N/2$. If the controlled time evolution is implemented in a straightforward manner [43], the number of two-qubit entangling gates is $20N\sigma/dt + 10N$. If instead we use the controlled reversal gate $\prod_{n \text{ even}} C_{Y_n}$, where the product of controlled- Y gates is over all even qubits, then only $N\sigma/dt + 2N$ two-qubit entangling gates are required. This is a roughly twenty-fold reduction in the number of gates. If we use the values $\sigma = 6$ and $dt = 0.2$, we arrive at $32N$ two-qubit entangling gates per rodeo cycle. In order for the peak probability to rise above the background value of $\frac{1}{2^n}$, the error rate per two-qubit entangling gate should be less than about $\frac{1}{64N}$. For an error rate of 0.3% we get $N \leq 5$, and for an error rate of 0.1% we get $N \leq 16$. Without controlled reversal gates, the corresponding values of N are reduced by a factor of twenty. This shows quite clearly the utility of the controlled reversal gates. We should mention that larger values of N are possible if high statistics with many Gaussian random times are used to make the background signal a smooth function of energy so that smaller peaks are also visible.

In addition to these constraints, we also need that the overlap between the initial state and eigenstate of interest is not much smaller than 1. One simple way to increase the initial state overlap is by using quantum adiabatic evolution as a preconditioner. This technique is discussed in Ref. [1].

-
- [1] K. Choi, D. Lee, J. Bonitati, Z. Qian, and J. Watkins, *Phys. Rev. Lett.* **127**, 040505 (2021), 2009.04092. 1, 4, 11
 - [2] A. M. Childs and N. Wiebe, *Quantum Info. Comput.* **12**, 901–924 (2012), ISSN 1533-7146. 2
 - [3] D. W. Berry, A. M. Childs, R. Cleve, R. Kothari, and R. D. Somma, in *Proceedings of the forty-sixth annual ACM symposium on Theory of computing* (2014), pp. 283–292.
 - [4] G. H. Low and I. L. Chuang, *Quantum* **3**, 163 (2019).
 - [5] A. Gilyén, Y. Su, G. H. Low, and N. Wiebe, in *Proceedings of the 51st Annual ACM SIGACT Symposium on Theory of Computing* (2019), pp. 193–204. 2
 - [6] S. Khatri, R. LaRose, A. Poremba, L. Cincio, A. T. Sornborger, and P. J. Coles, *Quantum* **3**, 140 (2019), ISSN 2521-327X, URL <https://doi.org/10.22331/q-2019-05-13-140>. 2
 - [7] B. K. Kamaka (2020).
 - [8] Y. S. Yordanov, D. R. M. Arvidsson-Shukur, and C. H. W. Barnes, *Phys. Rev. A* **102**, 062612 (2020), 2005.14475.
 - [9] B. Nash, V. Gheorghiu, and M. Mosca, *Quantum Science and Technology* **5**, 025010 (2020), URL <https://dx.doi.org/10.1088/2058-9565/ab79b1>.
 - [10] E. Younis and C. Iancu, in *2022 IEEE International Conference on Quantum Computing and Engineering (QCE)* (2022), pp. 465–475.
 - [11] E. E. Dobbs, J. S. Friedman, and A. Paler (2022), 2206.04990.
 - [12] M. Weiden, Younis, J. Kalloor, J. Kubiatoiwicz, and C. Iancu (2023), 2306.05622. 2
 - [13] G. Hao Low and I. L. Chuang, arXiv e-prints arXiv:1610.06546 (2016), 1610.06546. 2
 - [14] A. Y. Kitaev (1995), quant-ph/9511026. 2, 4

- [15] D. S. Abrams and S. Lloyd, *Phys. Rev. Lett.* **83**, 5162 (1999), quant-ph/9807070. 4
- [16] R. Cleve, A. Ekert, C. Macchiavello, and M. Mosca, *Proceedings of the Royal Society of London Series A* **454**, 339 (1998), quant-ph/9708016. 4
- [17] K. M. Svore, M. B. Hastings, and M. Freedman, *Quant. Inf. Comp.* **14**, 306 (2013), 1304.0741. 2, 4
- [18] M. Motta, C. Sun, A. T. Tan, M. J. O'Rourke, E. Ye, A. J. Minnich, F. G. Brandão, and G. K.-L. Chan, *Nature Physics* **16**, 205 (2020). 2
- [19] F. Turro, A. Roggero, V. Amitrano, P. Luchi, K. A. Wendt, J. L. DuBois, S. Quaglioni, and F. Pederiva, *Phys. Rev. A* **105**, 022440 (2022), 2102.12260. 2
- [20] R. M. Parrish and P. L. McMahon, arXiv e-prints arXiv:1909.08925 (2019), 1909.08925. 2
- [21] A. Francis, A. A. Agrawal, J. H. Howard, E. Kökcü, and A. F. Kemper, arXiv e-prints arXiv:2209.10571 (2022), 2209.10571. 3, 4
- [22] Y. Yang, Z. Zhang, X. Xu, B. Lu, and Y. Li, arXiv e-prints arXiv:2211.14854 (2022), 2211.14854.
- [23] C. L. Cortes and S. K. Gray, *Phys. Rev. A* **105**, 022417 (2022), 2109.06868.
- [24] C. Mejuto-Zaera and A. F. Kemper (2023), 2305.00060. 2, 3
- [25] E. Farhi, J. Goldstone, and S. Gutmann, arXiv preprint arXiv:1411.4028 (2014). 3
- [26] E. Farhi and A. W. Harrow, arXiv preprint arXiv:1602.07674 (2016).
- [27] L. Zhou, S.-T. Wang, S. Choi, H. Pichler, and M. D. Lukin, *Physical Review X* **10**, 021067 (2020). 3
- [28] W. Satula, J. Dobaczewski, W. Nazarewicz, and M. Rafalski, *Phys. Rev. C* **81**, 054310 (2010), 0912.4381. 3
- [29] J. M. Yao, B. Bally, J. Engel, R. Wirth, T. R. Rodríguez, and H. Hergert, *Phys. Rev. Lett.* **124**, 232501 (2020), 1908.05424.
- [30] J. A. Sheikh, J. Dobaczewski, P. Ring, L. M. Robledo, and C. Yannouleas, *J. Phys. G* **48**, 123001 (2021), 1901.06992.
- [31] M. Frosini, T. Duguet, J.-P. Ebran, B. Bally, T. Mongelli, T. R. Rodríguez, R. Roth, and V. Somà, *Eur. Phys. J. A* **58**, 63 (2022), 2111.00797.
- [32] E. A. Ruiz Guzman and D. Lacroix, *Phys. Rev. C* **105**, 024324 (2022), 2111.13080.
- [33] D. Lacroix, E. A. Ruiz Guzman, and P. Siwach, *Eur. Phys. J. A* **59**, 3 (2023), 2208.11567. 3
- [34] D. Frame, R. He, I. Ipsen, D. Lee, D. Lee, and E. Rrapaj, *Phys. Rev. Lett.* **121**, 032501 (2018), 1711.07090. 3
- [35] E. N. Epperly, L. Lin, and Y. Nakatsukasa, *SIAM J. Matrix Anal. Appl.* **43**, 1263 (2022), 2110.07492.
- [36] A. Sarkar, D. Lee, and U.-G. Meißner, *Phys. Rev. Lett.* **131**, 242503 (2023), 2306.11439.
- [37] T. Duguet, A. Ekström, R. J. Furnstahl, S. König, and D. Lee (2023), 2310.19419. 3
- [38] A. Smith, M. S. Kim, F. Pollmann, and J. Knolle, *npj Quantum Information* **5**, 106 (2019), ISSN 2056-6387, URL <https://doi.org/10.1038/s41534-019-0217-0>. 3
- [39] P. Siwach and D. Lacroix, *Phys. Rev. A* **104**, 062435 (2021), 2106.10867. 4
- [40] E. Farhi, J. Goldstone, S. Gutmann, and M. Sipser (2000), quant-ph/0001106. 4
- [41] N. Wiebe and N. S. Babcock, *New Journal of Physics* **14**, 013024 (2012). 4
- [42] Z. Qian, J. Watkins, G. Given, J. Bonitati, K. Choi, and D. Lee (2021), 2110.07747. 4, 7
- [43] M. S. Anis, Abby-Mitchell, H. Abraham, AduOffei, R. Agarwal, G. Agliardi, M. Aharoni, V. Ajith, I. Y. Akhalwaya, G. Aleksandrowicz, et al., *Qiskit: An open-source framework for quantum computing* (2021). 5, 11
- [44] M. Suzuki, *Proceedings of the Japan Academy, Series B* **69**, 161 (1993). 6, 11
- [45] N. Hatano and M. Suzuki, in *Lecture Notes in Physics, Berlin Springer Verlag*, edited by A. Das and B. K. Chakrabarti (2005), vol. 679, p. 37. 6, 11
- [46] Quantinuum, *Quantinuum H1-2* (March 9, 2022), URL <https://www.quantinuum.com/>. 7